ACSNANO
Cite This: ACS Nano XXXX, XXX, XXX−XXX
www.acsnano.org
ARTICLE

Label-Free Detection of Tear Biomarkers Using Hydrogel-Coated Gold Nanoshells in a Localized Surface Plasmon Resonance-Based Biosensor

Heidi R. Culver,[†,‡,#,▽] Marissa E. Wechsler,[†,‡,▽] and Nicholas A. Peppas*[,†,‡,§,∥,⊥]

[†]Institute for Biomaterials, Drug Delivery, and Regenerative Medicine, [‡]Department of Biomedical Engineering, [§]McKetta Department of Chemical Engineering, [∥]Division of Molecular Pharmaceutics and Drug Delivery, College of Pharmacy, and [⊥]Department of Surgery and Perioperative Care, Dell Medical School, The University of Texas at Austin, Austin, Texas 78712, United States

Supporting Information

ABSTRACT: The dependence of the localized surface plasmon resonance (LSPR) of noble-metal nanomaterials on refractive index makes LSPR a useful, label-free signal transduction strategy for biosensing. In particular, by decorating gold nanomaterials with molecular recognition agents, analytes of interest can be trapped near the surface, resulting in an increased refractive index surrounding the nanomaterial, and, consequently, a red shift in the LSPR wavelength. Ionic poly(*N*-isopropylacrylamide-*co*-methacrylic acid) (PNM) hydrogels were used as protein receptors because PNM nanogels exhibit a large increase in refractive index upon protein binding. Specifically, PNM hydrogels were synthesized on the surface of silica gold nanoshells (AuNSs). This composite material (AuNS@PNM) was used to detect changes in the concentration of two protein biomarkers of chronic dry eye: lysozyme and lactoferrin. Both of these proteins have high isoelectric points, resulting in electrostatic attraction between the negatively charged PNM hydrogels and positively charged proteins. Upon binding lysozyme or lactoferrin, AuNS@PNM exhibits large, concentration-dependent red shifts in LSPR wavelength, which enabled the detection of clinically relevant concentration changes of both biomarkers in human tears. The LSPR-based biosensor described herein has potential utility as an affordable screening tool for chronic dry eye and associated conditions.

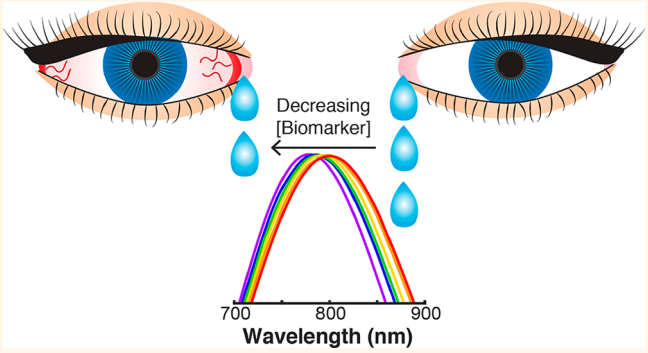

KEYWORDS: *localized surface plasmon resonance (LSPR), biosensor, hydrogel, gold nanoshell, protein biomarker, dry eye, label-free*

In the era of value-based healthcare, biosensors that are affordable, rapid, and easy to use are critical for medical decision making and appealing for point-of-care diagnostics.[1−3] However, traditional *in vitro* diagnostic tests do not meet these criteria because they often require specialized instrumentation for signal transduction and employ expensive molecular recognition agents (*e.g.*, antibodies).[4] The high cost of antibodies can make diagnostic tests prohibitively expensive, especially for complex diseases (*e.g.*, autoimmune disorders or cancer), where the detection of multiple biomarkers (*i.e.*, a "biomarker signature") is required to confirm the presence or absence of the disease.[5,6] To overcome this, lower cost alternatives for molecular recognition, such as aptamers[7−9] and synthetic polymers,[10,11] have been extensively investigated in recent years.

For example, many researchers have explored molecular imprinting as a route to develop synthetic polymers that selectively recognize and bind target molecules. The idea behind protein imprinting is that prior to polymerization protein molecules are combined with a set of monomers that form favorable interactions (electrostatic, hydrophobic, covalent, etc.) with the protein. After polymerization, the protein molecules are extracted, leaving a porous network with cavities complementary to the protein.[12] While the potential of protein imprinted polymers is alluring and remains a continued topic of research, there has been minimal success in achieving truly

Received: June 7, 2018
Accepted: September 11, 2018
Published: September 11, 2018

Downloaded via UNIV OF ALABAMA on September 24, 2018 at 13:07:47 (UTC).
See https://pubs.acs.org/sharingguidelines for options on how to legitimately share published articles.

© XXXX American Chemical Society

DOI: 10.1021/acsnano.8b04348
ACS Nano XXXX, XXX, XXX−XXX

Table 1. Comparison of LSPR-Based Biosensors Reported in the Literature Using Various Gold Nanomaterials and Recognition Agents

nanomaterial	recognition agent	immobilized or solution	max LSPR shift (nm)[a]	analyte	reference
silica-gold nanoshells	cross-linked hydrogel[b]	solution	50[c]	protein	this work
nanoantenna	cross-linked hydrogel[d]	immobilized	13	glucose	28
nanospheres	cross-linked hydrogel[e]	immobilized	3.8	protein	29
nanorods	organosiloxane MIP	immobilized	5	protein	30
nanorattles	organosiloxane MIP	immobilized	5	protein	31
nanorods	antibody	immobilized	3.5	protein	32
nanorods	antibody, peptide	immobilized	25	protein	33
silver-gold nanoshells	antibody, biotin−avidin	immobilized	15	protein	34
nanorods	antibody, biotin−avidin	immobilized	3	protein	35
nanospheres	antibody, biotin−avidin	immobilized	9.3	virus	36
nanostars	antibody, biotin−avidin	solution	30 (80[f])	protein	26
nanospheres	glycopolymer	solution	53[f]	protein	27

[a]Maximum shift from λ_{LSPR} of receptor-coated nanomaterial. [b]Monomers: *N*-isopropylacrylamide, methacrylic acid, and *N*,*N*′-methylenebis(acrylamide) (electrostatic attraction). [c]For both lactoferrin and lysozyme in tears at a concentration of 196 μg/mL. [d]Monomers: hydroxyethyl methacrylate, *N*-3-acrylamidophenylboronic acid, and ethylene glycol dimethacrylate (boronic acid-diol). [e]Monomers: acrylamide and *N*,*N*′-methylenebis(acrylamide) (diffusion, nonspecific). [f]Shift as a result of both refractive index change and plasmon coupling.

selective polymers, largely due to challenges associated with protein size and structural complexity.[13−15]

Given the extra time and costs associated with preparing protein imprinted polymers without substantially improving selectivity, nonimprinted hydrogels capable of semiselective protein recognition are appealing alternatives. For example, several groups have demonstrated the utility of poly(*N*-isopropylacrylamide) (PNIPAM)-based hydrogels to capture and concentrate protein biomarkers.[16−18] PNIPAM-based hydrogels are unique thermoresponsive polymers that exhibit a lower critical solution temperature (LCST) around 31 °C.[19] At temperatures below the LCST, PNIPAM hydrogels are highly swollen, whereas at temperatures above the LCST, the polymer gels undergo hydrophobic collapse. The highly swollen nature of PNIPAM gels at room temperature is a critical feature for the diffusion of solutes into and throughout the polymer network. For example, we recently demonstrated that anionic poly(*N*-isopropylacrylamide-*co*-methacrylic acid) (PNM) nanogels exhibit affinity and high adsorption capacity for high isoelectric point (pI) proteins due to favorable electrostatic interactions between the negatively charged polymer and positively charged proteins. Additionally, the affinity for different proteins was tuned by changing the ionizable groups present in the nanogels as well as the buffer in which binding was performed.[20]

Conveniently, these nanogels also served as signal transduction agents. For highly swollen PNM nanogels, protein binding throughout the nanogel increased the refractive index mismatch between the nanogels and buffer and, consequently, increased turbidity. Turbidity is a function of both particle concentration and refractive index mismatch.[21] To maximize turbidity, there is an obvious trade-off: increasing the nanogel concentration decreases the number of proteins bound per nanogel, which, in turn, decreases the refractive index change per nanogel. This trade-off between particle concentration and refractive index mismatch limits the signal intensity (*i.e.*, change in turbidity) at low protein concentrations, making it difficult to achieve low detection limits.

To overcome this limitation and achieve better sensitivity, we hypothesized that PNM nanogels could be used in a localized surface plasmon resonance (LSPR)-based biosensor. LSPR occurs when the conduction electrons of noble-metal nanomaterials collectively oscillate upon interaction with light.[22,23] The result is strong absorbance of light of a specific wavelength, which depends on the geometry of the nanomaterial and, importantly, the refractive index of the surrounding medium.[24] Unlike in turbidimetry (an intensiometric method), in LSPR-based sensing (a colorimetric method), signal magnitude is not a direct function of particle concentration. Rather, for a given analyte concentration, LSPR shifts generally increase with decreasing particle concentration (as long as the optical density of the gold nanomaterial is detectable and the concentration of receptors is above the dissociation constant), because the largest refractive index mismatch is achieved when the binding sites on each particle are saturated. To reach saturation at low protein concentrations, a low particle concentration is needed. Thus the fact that LSPR signal magnitude is not positively correlated to particle concentration is a useful attribute for achieving low detection limits and makes LSPR a powerful "label-free" tool for biomarker detection.[23,25]

In this work, an LSPR-based biosensor for protein detection was developed using PNM-coated silica gold nanoshells (AuNSs) (AuNS@PNM). Compared with previously reported LSPR biosensors, the biosensor developed herein exhibits LSPR shifts of unprecedented magnitude (up to 50 nm) upon analyte binding (Table 1). The large LSPR shifts were attributed to the high refractive index sensitivity of AuNSs in combination with the high swellability of PNM, which enables high analyte adsorption capacity and drastic changes in refractive index. In the few other reports where analyte-induced shifts >50 nm were observed,[26,27] the large shifts were achieved by a combination of analyte-induced refractive index changes and plasmon coupling, the latter of which relies on multivalent interactions between ligands and receptors. In contrast, the large LSPR shifts observed in this work were solely attributed to refractive index changes. Additionally, unlike many of the previously developed LSPR-based biosensors, the solution-based nature of the current sensor enables assay performance in routine plate readers rather than requiring specialized setups (Table 1).

Herein we demonstrate the utility of AuNS@PNM composite nanomaterials as LSPR-based biosensors for detecting changes in the concentration of two protein

DOI: 10.1021/acsnano.8b04348
ACS Nano XXXX, XXX, XXX−XXX

biomarkers for chronic dry eye: lysozyme and lactoferrin. Compared with the healthy population, lysozyme and lactoferrin concentrations are significantly lower in patients with chronic dry eye and associated conditions.[37−39] Despite the high prevalence of dry eye, it is frequently underrecognized and impacts patients' vision and quality of life.[40] Currently, dry-eye diagnosis is based on several tests to evaluate the ocular surface and tear film production.[40−42] While these tests are standard and necessary diagnostic approaches, many researchers have reported the need for identification, validation, and detection of tear biomarkers to assist in reaching a conclusive diagnosis.[42−44] Commercially available assays that are used to monitor select tear biomarker concentrations include enzyme-linked immunosorbent assays (ELISAs),[42] Advanced Tear Diagnostics' TearScan Lactoferrin Diagnostic Test Kit,[45] and Quidel Corporation's InflammaDry, a test for elevated MMP-9.[46] Unfortunately, these methods require specialized equipment (in the case of the TearScan Microassay System) or antibodies (used for ELISAs and InflammaDry), which have poor environmental stability and are relatively expensive.[4,47]

The LSPR-based biosensor developed herein overcomes these limitations by using a single synthetic receptor to detect clinically relevant lysozyme and lactoferrin concentration changes in tears. The materials and signal transduction method used in this biosensor are low-cost, the performance of the test requires only a few microliters of tears, and the test can be completed within minutes using a routine plate reader. Further testing using samples from dry-eye and non-dry-eye patients will validate the potential utility of the developed biosensor as an affordable and rapid screening tool for chronic dry eye.

RESULTS AND DISCUSSION

Synthesis and Characterization of Silica-Gold Nanoshells. The LSPR wavelength of gold nanomaterials depends on the size and shape of the nanomaterial, as well as local refractive index.[24] Nanomaterials with red-shifted LSPR wavelengths enhance biosensor performance because they have increased sensitivity to local refractive index compared to nanomaterials with lower LSPR wavelengths.[48] One way to red-shift the LSPR wavelength is to increase the aspect ratio of the nanomaterial.[23] For example, high aspect ratio nanorods and nanostars both exhibit red-shifted LSPR.[49,50] However, both of these nanomaterials are also anisotropic, giving rise to plasmonic "hot spots," where the plasmon resonance is stronger and more sensitive.[51]

For gold nanorods (AuNRs), the "hot spots" are located at the tips because the longitudinal plasmon resonance is stronger and much more sensitive than the transverse plasmon resonance.[30] However, the surface area of the ends is small relative to the surface area of the sides, so for uniformly coated AuNRs, the majority of the protein will be bound on the sides, where the plasmon resonance is less sensitive. There are two ways to overcome this challenge: develop a method to favor binding at the ends of the AuNRs[30,52] or use isotropic nanomaterials with a comparable refractive index sensitivity to the longitudinal plasmon resonance of AuNRs.[53] On the basis of previous reports,[54] we expected that silica core-gold nanoshells (AuNSs) would meet the criteria for the second approach and thus were chosen as the gold nanomaterial cores in this work.[55] Although AuNSs have appealing properties for biosensing, there are few reports of silica gold nanoshells being used in solution-based LSPR biosensors.

The successful formation of AuNSs with $\lambda_{LSPR} \approx 780$ nm was determined by absorbance spectroscopy, transmission electron microscopy (TEM), and dynamic light scattering (DLS) (Figure 1 and Table S1). The refractive index

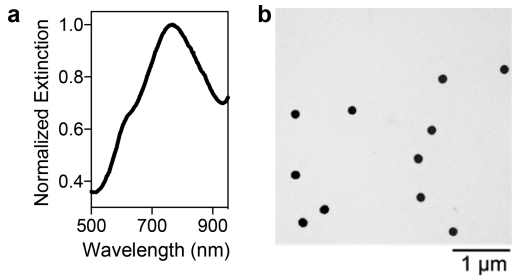

Figure 1. Characterization of AuNS synthesis. (a) Extinction spectrum of well-formed AuNSs showing a peak-to-trough ratio around 3 and shoulder around 600 nm. (b) TEM image of bare AuNSs.

sensitivity of AuNSs ($\lambda_{LSPR} \approx 780$ nm) was then compared to that of spherical colloidal gold (AuNPs) ($\lambda_{LSPR} \approx 520$ nm). Specifically, both nanomaterials were suspended in solutions of various weight percent sucrose, which have well-characterized refractive indices.[56] Figure 2 shows the clear improvement in

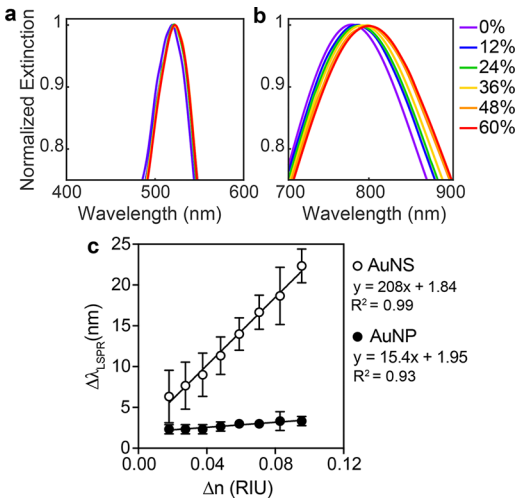

Figure 2. Refractive index sensitivity of AuNSs compared with AuNPs. Gaussian fits to LSPR peaks of (a) AuNPs and (b) AuNSs suspended in solutions of varying weight percent sucrose with known refractive indices. (c) Shifts in LSPR as a function of change in refractive index for AuNSs and AuNPs. AuNSs exhibited greater refractive index sensitivity (210 nm/RIU) compared with AuNPs (17.4 nm/RIU).

LSPR sensitivity for the AuNSs relative to AuNPs. AuNSs exhibited a refractive index sensitivity of 210 nm/RIU, which is comparable to refractive index sensitivities previously reported for the longitudinal plasmon resonance of AuNRs (170−325 nm/RIU),[32,53,57] whereas AuNPs had a refractive index sensitivity of only 17.4 nm/RIU. This improved sensitivity means that for the same concentration of bound protein (y axis of Figure 2F should read the same as Figure 2G, same refractive index change), a significantly larger shift in LSPR would be expected for AuNSs relative to AuNPs.

Synthesis and Characterization of Hydrogel-Coated Gold Nanoshells. Gold-PNIPAM composite materials have

DOI: 10.1021/acsnano.8b04348
ACS Nano XXXX, XXX, XXX−XXX

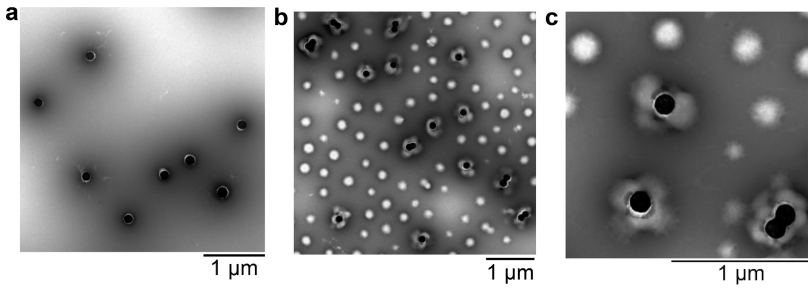

Figure 3. TEM characterization of AuNS@PNM. (a) TEM image of DDT-capped, PMAO-*g*-PEGMA-stabilized AuNSs. (b,c) TEM images showing a mixture of coreless PNM nanogels and AuNS@PNM with flower-like architecture at (b) 16 500× and (c) 43 000×. All samples were stained with 2% phosphotungstic acid (pH 7.0).

been extensively explored for a variety of applications,[58] including photothermal therapy,[59,60] temperature sensing,[61−66] catalysis,[67,68] and thermally activated optical switching.[69,70] However, despite the favorable protein binding properties of PNIPAM gels, the use of gold-PNIPAM composites in protein biosensing applications has not been extensively explored.

To synthesize PNM on the surface of the AuNSs, the AuNSs were first modified with 1-dodecanethiol (DDT) and then stabilized by an amphiphilic graft copolymer, poly(maleic anhydride-*alt*-1-octadecene)-*g*-poly(ethylene glycol methacrylate) (PMAO-*g*-PEGMA) *via* solvent displacement.[71] PMAO-*g*-PEGMA has pendant methacrylate groups that can be used to anchor the growing polymer chains to the surface of the AuNSs. Modification with PMAO-*g*-PEGMA resulted in red-shifted LSPR and an increase in hydrodynamic diameter and zeta potential (Table S1). The DDT and PMAO-*g*-PEGMA layer was visualized by TEM (Figure 3a).

The synthesis of PNM shells was achieved by following previously reported precipitation polymerization protocols, except PMAO-*g*-PEGMA-stabilized AuNSs were included in the reaction mixture.[20] TEM imaging revealed AuNSs with polydisperse, flower-like PNM shells (Figure 3b,c). The polydispersity of the PNM shells was greater than PNM nanogels synthesized in the absence of AuNSs, which was primarily attributed to the opposing effects of pH on PNM growth and PMAO-*g*-PEGMA stability. Specifically, the polymerization was done at a low pH (∼3.8), where methacrylic acid is mostly protonated so that PNM readily undergoes hydrophobic collapse, resulting in uniform nanogel size. However, the solubility of PMAO-*g*-PEGMA is improved at pH values above the pK_a of its pendant carboxylic acids (∼4 to 5), resulting in some instability at the polymerization pH. The flower-like architecture of AuNS@PNM is likely a result of PNM nucleation in solution (as evidenced by the many PNM nanogels without AuNS cores) and subsequent reaction with the methacrylate groups on the PMAO-*g*-PEGMA-stabilized AuNSs (Figure 4). Using this graft-to approach, it is not surprising that multiple nanogels anchored to each AuNS. Prior to use in LSPR studies, PNM nanogels without AuNS cores were removed from AuNS@PNM *via* multiple rounds of centrifugation and resuspension in nanopure water.

Investigation of Factors Affecting LSPR Shifts. In designing AuNS@PNM for protein biosensing, it was critical to consider what factors would influence shifts in LSPR. The magnitude of refractive index change upon protein binding to a surface can be described by the De Feijter equation[72]

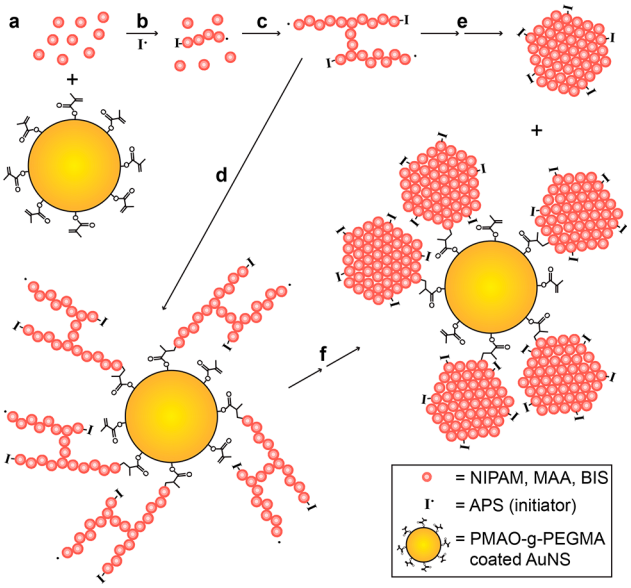

Figure 4. Schematic depiction of the process expected to lead to the AuNS@PNM flower-like architecture. (a) Monomers, *N*-isopropylacrylamide (NIPAM), methacrylic acid (MAA), and *N*,*N*′-methylenebis(acrylamide) (BIS) (pink spheres) were mixed with PMAO-*g*-PEGMA-stabilized AuNSs (gold spheres). (b) Upon initiation with ammonium persulfate (APS, I·) at 70 °C, polymer chains grow, (c) eventually cross-linking with other oligomers in solution, and (d) reacting with the methacrylate groups on the PMAO-*g*-PEGMA-stabilized AuNSs. Upon reaching a critical size, the growing networks undergo hydrophobic collapse because of the LCST response of PNIPAM copolymers, resulting in both (e) coreless PNM nanogels and (f) AuNS@PNM flower-type structures. The presence of anionic sulfate groups (from APS) on the surface results in colloidally stable PNM nanogels and AuNS@PNM composites.

$$\Delta n = \frac{\theta\left(\frac{dn}{dc}\right)}{d_A}$$

where Δn is the difference in refractive index between the protein and buffer, θ is the adsorbed surface mass density (g/cm^2), d_A is the thickness of the adsorbed layer (cm), and dn/dc is the refractive index increment of the protein (a typical value for protein adsorption is 0.186 cm^3/g).[73] From this equation, it is clear that the magnitude of the change in refractive index and corresponding shift in LSPR depend on both the adsorbate thickness and the amount of protein that binds. Whereas the PNM shells made *via* precipitation polymerization were not thin or uniform, the highly swollen structure that resulted from

DOI: 10.1021/acsnano.8b04348
ACS Nano XXXX, XXX, XXX−XXX

this method is beneficial for rapid diffusion of proteins into the nanogel network. The sensitivity of the biosensor could potentially be improved in future work by exploring approaches for growing thinner, more uniform nanogels on the AuNSs, such as through inverse microemulsion polymerization[74] or surface-initiated controlled ATRP or RAFT polymerization.[75−77] However, achieving thin shells should not be prioritized over achieving high swellability.

In the current work, we focused on characterizing the LSPR sensitivity of AuNS@PNM to the amount of bound protein. The dependence of the refractive index change on amount of protein bound is critical for our protein biomarker sensing strategy (Figure 5). On the basis of the De Feijter equation, it

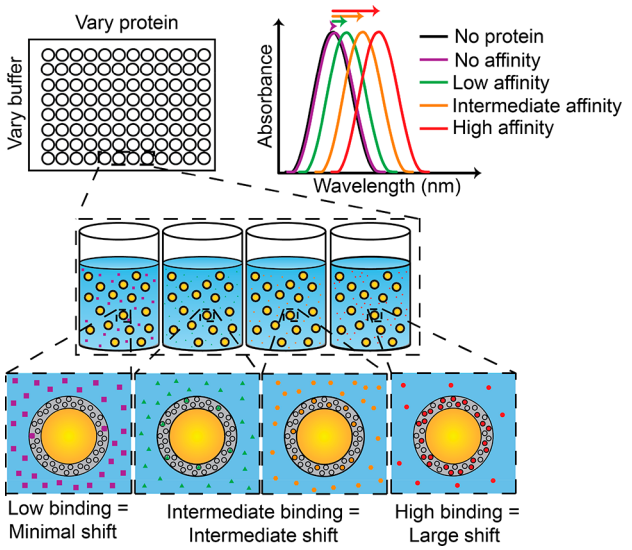

Figure 5. Schematic depiction of LSPR-based biosensor. For low-affinity interactions or low protein concentrations, little to no shift in LSPR wavelength is expected. As protein concentration or affinity increases, larger red shifts in LSPR wavelength are expected.

was expected that shifts in LSPR would be dependent on both protein concentration as well as the affinity of PNM for proteins in different buffers. For example, for low-affinity protein−polymer interactions, little to no shifts in LSPR were expected, whereas for high-affinity interactions, large red shifts were expected due to the increased refractive index upon protein binding.

In our previous paper, we showed that PNM had high affinity for high-pI proteins but low affinity for near-neutral or low-pI proteins in 0.1× phosphate-buffered saline (pH 7.4) due to favorable and unfavorable electrostatic interactions, respectively.[20] Thus it was expected that only high-pI proteins, but not low- or near-neutral-pI proteins, would cause shifts in LSPR when binding was performed at pH 7.4. To confirm this, binding studies were performed with lysozyme (pI ∼11.3), myoglobin (pI ∼7.0), and ovalbumin (pI ∼4.5). Indeed, incubation with lysozyme caused detectable red shifts in the LSPR wavelength at concentrations above 1000 nM ($p < 0.05$), whereas incubation with myoglobin or ovalbumin did not (Figure 6 and Figure S1). Overall, these results confirm that the extent of protein binding is dictated by protein concentration and electrostatic interactions between PNM nanogels and proteins.

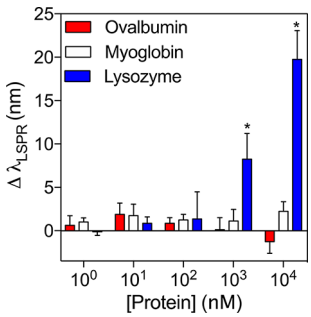

Figure 6. Dependence of LSPR shifts on protein isoelectric point (pI). Quantitative analysis of LSPR shifts of AuNS@PNM with increasing concentrations of ovalbumin (pI ∼4.5), myoglobin (pI ∼7.0), or hen egg white lysozyme (pI ∼11.3) in 0.1× PBS. No significant changes in LSPR wavelength were observed upon incubation of AuNS@PNM with ovalbumin or myoglobin. However, significant shifts in LSPR wavelength were observed upon incubation of AuNS@PNM with lysozyme at concentrations above 1000 nM. Data are presented as mean ± SD (n = 4, Student's t test, $*p < 0.05$).

Characterization of Buffer Effect and Semiselectivity. After demonstrating that the AuNS@PNM biosensor was able to bind lysozyme to produce concentration-dependent LSPR shifts, we next sought to test the cross-reactivity of AuNS@PNM for another high-pI protein biomarker of dry eye, lactoferrin. Specifically, we measured the LSPR shifts induced by lactoferrin and lysozyme across a wide range of concentrations in 0.1× phosphate-buffered saline (hereafter referred to simply as PBS) and 0.1× histidine-buffered saline at pH 5.5 (hereafter referred to simply as HBS). We chose to use both PBS and HBS because, based on our previous findings,[20] the adsorption capacity (*i.e.*, mass of protein bound per mass of PNM) of lysozyme to PNM is higher than lactoferrin in PBS, but lower than in HBS. Thus we hypothesized that the buffer identity would affect the magnitude of protein binding-induced LSPR shifts for both lysozyme and lactoferrin.

Whereas lysozyme binding caused similar responses in both buffers (Figure 7a), lactoferrin binding caused significantly larger LSPR shifts in HBS than in PBS at concentrations above 100 nM ($p < 0.05$) (Figure 7b). Improved binding of lactoferrin to AuNS@PNM in HBS was attributed to an increase in overall charge and improved solubility of lactoferrin at pH 5.5 (*i.e.*, in HBS) compared to pH 7.4 (*i.e.*, in PBS). We also suspect that lactoferrin caused larger shifts in LSPR than lysozyme in HBS because for the same molar concentration, the mass concentration of lactoferrin (MW ≈ 83 kDa) is nearly six times higher than that of lysozyme (MW ≈ 14 kDa). Conversely, lysozyme binding was favored at high pH due to the loss of charge on lactoferrin (pI ∼8.8) compared with lysozyme (pI ∼11.3). Overall, these results demonstrate the cross-reactivity of AuNS@PNM for high-pI proteins and that buffer pH influences binding affinity by changing the relative charge of the two proteins.

Determination of the Useful Dynamic Range in Buffer. Having tested the LSPR response of AuNS@PNM upon incubation with a wide range of lysozyme and lactoferrin concentrations, the next step was to test concentration-dependent LSPR shifts over a narrower, clinically relevant range of concentrations. Healthy concentrations of lysozyme and lactoferrin in tears typically span a range of ∼1−3 mg/mL, with an average concentration of 2 mg/mL for both proteins.

DOI: 10.1021/acsnano.8b04348
ACS Nano XXXX, XXX, XXX−XXX

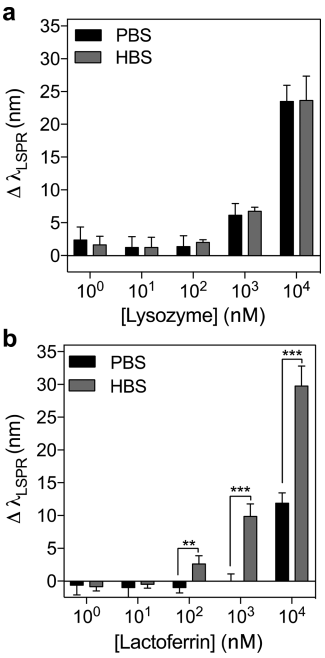

Figure 7. Quantification of AuNS@PNM LSPR shifts for lysozyme and lactoferrin across a wide range of concentrations. (a) For lysozyme, shifts in LSPR were similar in both buffers (PBS or HBS) for all concentrations tested. (b) For lactoferrin, shifts in LSPR were significantly higher in HBS than in PBS for the three highest concentrations tested. Data are presented as mean ± SD (n = 4, Student's t test, $^{**}p < 0.01$, $^{***}p < 0.001$).

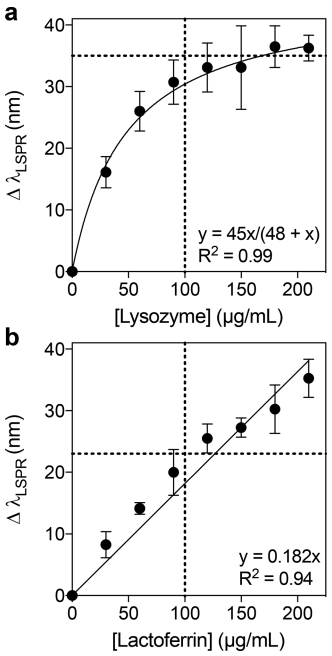

Figure 8. Quantification of LSPR shifts for lysozyme and lactoferrin in HBS. The magnitudes of shifts in LSPR of AuNS@PNM upon incubation with either lysozyme or lactoferrin. (a) For lysozyme, LSPR was more sensitive at low protein concentrations and then plateaued at high concentrations. (b) For lactoferrin, shifts in LSPR increased linearly with protein concentration. Data are reported as mean ± SD (n = 4).

Concentrations <1 mg/mL are often associated with chronic dry eye,[39,42] but other factors (*e.g.*, patient age[78] and tear collection method[43,79]) affect protein concentrations, necessitating the use of age-matched controls and standardized sample collection methods in clinical diagnostic settings. In general, the high abundance of lysozyme and lactoferrin in tears makes them convenient targets for diagnostics because just a few microliters of tears can be collected and diluted for use in a biosensor. This is important because collecting large volumes of tears is difficult, particularly for patients with dry eye.[43] To minimize the volume of tears needed for use in our LSPR-based biosensor, all experiments were performed in 384-well plates.

Before testing the LSPR response of AuNS@PNM in tears, the LSPR shifts of each protein were measured in simple, noncompetitive (*i.e.*, single protein) experiments. Solutions of human lysozyme and lactoferrin were prepared at concentrations that were expected to correspond to that of a 1/10 dilution of tears. At this dilution, the average healthy tear concentration would be ∼200 μg/mL, and the upper cutoff concentration for healthy *versus* dry-eye patients would be ∼100 μg/mL. In buffer (HBS) alone, concentration-dependent LSPR shifts were observed for both proteins. Lysozyme caused larger shifts in LSPR at lower protein concentrations and plateaued after 100 μg/mL (Figure 8a), whereas lactoferrin showed a nearly linear response (Figure 8b). On the basis of these data, LSPR shifts of 35 (for lysozyme) or 23 nm (for lactoferrin) would correspond to the cutoff concentration for healthy *versus* dry-eye patients (∼100 μg/mL). For lysozyme, dilutions >1/10 could be used to stay below saturation and better differentiate healthy *versus* dry-eye concentrations. Overall, these data demonstrate the ability of AuNS@PNM to respond to changes in protein biomarker concentration over a range relevant to the diagnosis of chronic dry-eye conditions.

Determination of the Useful Dynamic Range in Diluted Human Tears. Whereas the previous noncompetitive studies were informative, it was necessary to demonstrate biomarker binding in tears to better demonstrate applicability as a dry-eye biosensor. Lysozyme, lactoferrin, lipocalin, and secretory IgA make up the majority of the protein content in tears.[80,81] Of these proteins, lysozyme and lactoferrin are high-pI proteins, whereas lipocalin and IgA have pIs below neutral (Table 2). Because the LSPR biosensor developed in this work detects proteins based on electrostatic interactions (Figure 6), anionic AuNS@PNM will preferentially bind lysozyme and lactoferrin (high concentration and high pI). Thus lipocalin and IgA (high concentration but low pI), in addition to other tear proteins, which are present at much lower concentrations (Table 2), are not expected to interfere with binding or significantly contribute to the LSPR signal.

The concentrations of lactoferrin and lysozyme in the pooled human tears used for the remaining studies were found to be 3.8 and 1.9 mg/mL, respectively, by ELISA (Figure S2). The unexpectedly high concentration of lactoferrin may be attributed to the collection method used (collection from crying/watering eyes), evaporative concentration during processing and handling, or other unknown variables (*e.g.*, age and health of donors). If translated to the clinic, sample collection and handling would be standardized, and the biosensor would need to be further trained using tear samples from dry-eye patients and age-matched controls to ensure diagnostic accuracy.

In the current study, pooled human tears were diluted in either HBS or PBS to achieve baseline lysozyme and lactoferrin concentrations of 16 μg/mL. Because of the high concen-

DOI: 10.1021/acsnano.8b04348
ACS Nano XXXX, XXX, XXX−XXX

Table 2. Protein Composition and Concentrations in Healthy Human Tears

protein	pI	concentration (healthy) (μg/mL)	ref
lysozyme	11.3	$2.0 \pm 1.0 \times 10^3$	39
lactoferrin	8.7	$2.0 \pm 1.1 \times 10^3$	39
lipocalin-1	5.3	$1.7 \pm 0.5 \times 10^3$	82
sIgA	4.5−6.5	$1.7 \pm 0.7 \times 10^3$	80
ZA2G	5.7	$4.3 \pm 2.4 \times 10^2$	82
IgM	4.5−6.5	$1.8 \pm 0.5 \times 10^1$	83
transferrin	5.6, 5.2	$1.6 \pm 0.3 \times 10^1$	83
albumin	4.7	$1.2 \pm 0.8 \times 10^1$	80
IgG	6.5−9.5	$3.6 \pm 0.6 \times 10^0$	83
IgE	varies	$2.2 \pm 2.0 \times 10^{-2}$	84
IL-8	9.1	$1.7 \pm 0.3 \times 10^{-2}$	85
EGF	4.6	$5.1 \pm 3.7 \times 10^{-3}$	86
IL-6	6.2	$6.3 \pm 1.7 \times 10^{-4}$	85
IL-1β	4.6	$4.4 \pm 1.2 \times 10^{-4}$	85
INF-γ	9.5	$2.8 \pm 0.5 \times 10^{-4}$	85
IL-4	8.2	$2.6 \pm 0.9 \times 10^{-4}$	85
IL-10	8.5	$2.6 \pm 0.6 \times 10^{-4}$	85
TNF-α	5.3	$2.5 \pm 0.6 \times 10^{-4}$	85
IL-5	7.8	$1.6 \pm 0.4 \times 10^{-4}$	85
IL-18	8.3	$1.1 \pm 0.3 \times 10^{-4}$	87
Aquaporin5	8.8	$3.1 \pm 2.4 \times 10^{-5}$	86

trations of lysozyme and lactoferrin in tears, diluting tears by a factor of 10^3 to 10^5 is common practice prior to performing commercial tests for these proteins (*i.e.*, ELISAs, Advanced Tear Diagnostics' TearScan Lactoferrin Diagnostic Test Kit). The dilution of tears for dry-eye diagnostics not only achieves biomarker concentrations within the dynamic range but also is necessary to increase the sample volume (because individuals with dry eye have abnormally low tear production) and to modulate conditions of the aqueous medium. Through this step, the pH and ionic strength can be controlled to promote optimal conditions for specific analyte interaction with the receptors.

Control over pH and ionic strength is particularly important for the AuNS@PNM LSPR sensor developed here because variations in temperature, pH, and ionic strength affect the swelling behavior of PNM nanogels, which, in turn, can affect protein diffusion into the network and the LSPR response of the sensor. Dynamic light scattering studies demonstrated that PNM nanogels at pH 7.4 (*i.e.*, in PBS) were more sensitive to changes in ionic strength than nanogels at pH 5.5 (*i.e.*, in HBS) but were less sensitive to temperature (Figure S3). This can be explained by the fact that there is a higher percentage of deprotonated carboxylic acid groups at pH 7.4 than pH 5.5, which prevents hydrophobic collapse above the LCST of PNIPAM and makes the degree of swelling more dependent on ionic strength. These results underscore the importance of dilution into a buffer with known ionic strength and pH prior to using the AuNS@PNM biosensor for the detection of protein biomarkers.

After diluting the tears to baseline levels (*i.e.*, 16 μg/mL) of lysozyme or lactoferrin, concentrated stock solutions of human lysozyme or lactoferrin were spiked into the diluted tears to increase the biomarker concentrations by 20 μg/mL increments up to 216 μg/mL. Spiking known concentrations of analyte into a matrix with other components of unknown concentration is the most common method for preparing samples for method validation.[88] Lysozyme or lactoferrin concentrations were first varied individually to study the effect of each protein on the LSPR of AuNS@PNM. The magnitude of the observed LSPR shifts was affected by variations in protein concentrations, as well as which buffer was used for the assay (Figure 9).

For each experiment, a distinct "cutoff concentration" was observed, above which the LSPR response was not statistically different from higher concentrations tested. In the bar graphs shown in Figure 9, concentrations above the "cutoff concentration" were binned into a single group for clarity. Shifts in LSPR for all protein concentrations tested are shown in Table S2. The range from the lowest concentration to the "cutoff concentration" is considered the dynamic range. Whether a narrow or wide dynamic range is better depends on the intended application: Sensors with narrow dynamic ranges have good sensitivity (*i.e.*, steep relationship between analyte concentration and signal magnitude), whereas sensors

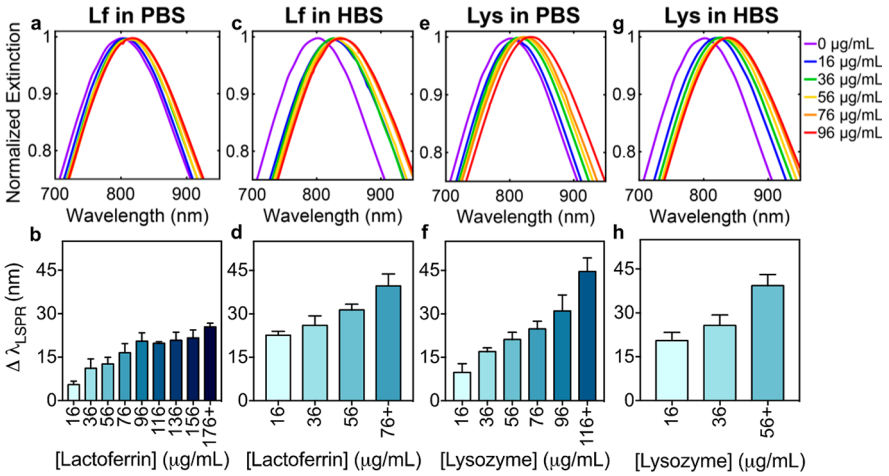

Figure 9. Analysis of LSPR shifts upon variation of individual biomarker concentration in human tears. Gaussian fits to LSPR peaks of AuNS@PNM normalized extinction spectra and quantitative analysis of shifts in LSPR of AuNS@PNM with increasing concentrations of (a−d) lactoferrin (Lf) or (e−h) lysozyme (Lys) in either PBS or HBS. For clarity, Gaussian fits for high concentrations (*i.e.*, >96 μg/mL) were omitted. Quantitative analysis of shifts in LSPR in PBS for both proteins (b,f) showed a larger dynamic response across the concentrations tested compared with a narrower dynamic response range observed in HBS (d,h). Data are reported as mean ± SD ($n \geq 3$).

DOI: 10.1021/acsnano.8b04348
ACS Nano XXXX, XXX, XXX−XXX

with wide dynamic ranges allow analyte detection over a larger concentration range.[89]

LSPR shifts observed upon lactoferrin binding in tears diluted in PBS (Figure 9a,b) were smaller in magnitude than LSPR shifts in HBS diluted tears (Figure 9c,d). As previously mentioned, this can be explained by the increased charge and improved solubility of lactoferrin at pH 5.5 (*i.e.*, in HBS) compared to pH 7.4 (*i.e.*, in PBS), resulting in increased binding of lactoferrin to AuNS@PNM. The magnitude of shifts in LSPR upon lysozyme binding to AuNS@PNM was comparable in both buffers at intermediate concentrations (96−176 μg/mL). However, at low concentrations (≤76 μg/mL), shifts in LSPR were significantly smaller in PBS than in HBS, whereas at high concentrations shifts in LSPR were significantly larger in PBS ($p < 0.05$) (Figure 9e−h). This is likely a result of decreased swelling of PNM in HBS compared with in PBS (Figure S3), which limits protein diffusion into and binding throughout the nanogel.

The overall biosensor performance in both buffers was also compared. For both proteins, the analysis of LSPR shifts in PBS (Figure 9b,f) showed a dynamic response across a wider range of the concentrations tested compared with a narrower dynamic range observed in HBS (Figure 9d,h). For lactoferrin, this is attributed to the higher affinity between PNM and the protein in HBS compared with that in PBS, resulting in binding saturation at lower concentrations in HBS. For lysozyme, the decreased dynamic range observed in HBS was attributed primarily to increased competition with lactoferrin for binding sites in HBS compared to in PBS. Specifically, the baseline level of lactoferrin in the tears (32 μg/mL) occupies more of the available binding sites in HBS than in PBS, as evidenced by the significantly larger shifts in LSPR in HBS (23 ± 0.7 nm) compared to that in PBS (5.5 ± 0.7 nm) ($p < 0.001$). Additionally, binding to near-neutral pI proteins present at moderately high concentrations in tears, such as immunoglobulins (Table 2), is possible in HBS and could have also contributed to the narrow dynamic range (*i.e.*, large LSPR shifts and saturation at low biomarker concentrations). On the basis of our previous results,[20] it is unlikely that near-neutral pI proteins will bind AuNS@PNM in PBS, hence the wider dynamic range and lower initial LSPR shifts. The ability to tune both the dynamic range and the magnitude of the LSPR responses by varying the buffer improves the versatility and utility of AuNS@PNM for protein biosensing.

LSPR Response to Simultaneous Variation of Both Biomarker Concentrations. Next, to test the impact of cross-reactivity for lysozyme and lactoferrin on the sensor performance, concentrations of both biomarkers were varied simultaneously to better represent the competitive environment expected in real patient tears. On the basis that lysozyme and lactoferrin binding to AuNS@PNM is driven by electrostatic interactions, there will undoubtedly be cross-reactivity and competition between these two biomarkers when they are present at similar concentrations. However, competition with other high-pI proteins is not expected to be significant because the concentration of these proteins in tears is two to eight orders of magnitude lower than the concentrations of lysozyme and lactoferrin (Table 2).

The LSPR shifts of AuNS@PNM when each protein was varied individually were compared to the LSPR shifts for simultaneous variation, both measured and hypothetical (*i.e.*, if there was no competition and sufficient binding sites for both proteins) (Figure S4). In cases where protein concentrations are sufficiently low, there are enough binding sites to accommodate both proteins, thus minimizing competition. In these cases, there should not be a statistical difference between the measured and hypothetical LSPR shifts. In PBS, this was only true when the concentration of both proteins was ≤76 μg/mL, whereas in HBS, the hypothetical LSPR shifts were larger than the measured shifts for all concentrations tested.

When the concentrations of both proteins were each ≥96 μg/mL in PBS, the measured shifts were not statistically different from the lysozyme-only shifts. On the basis of previous studies, where we found that carboxylic-acid-containing hydrogels preferentially bind lysozyme over other high-pI proteins in competitive environments because of its particularly high pI and uniquely large arginine-to-lysine ratio, we hypothesized that AuNS@PNM preferentially bound lysozyme over lactoferrin in PBS.[14] However, in HBS, the LSPR shifts observed when both proteins were varied simultaneously were not statistically different than the shifts caused by either lysozyme or lactoferrin alone at most concentrations >96 μg/mL (Figure S4), suggesting increased competition in this buffer.

Figure 10 shows the sensor response to simultaneous biomarker variation, focusing on the dynamic range. It was not surprising that when both biomarker concentrations were varied simultaneously the dynamic range was narrower in both PBS (Figure 10a,b) and HBS (Figure 10c,d) compared with when the biomarkers were varied individually (Figure 9). The dilution factor and best buffer(s) in which to dilute tears for optimal sensor performance will be elucidated when the sensor

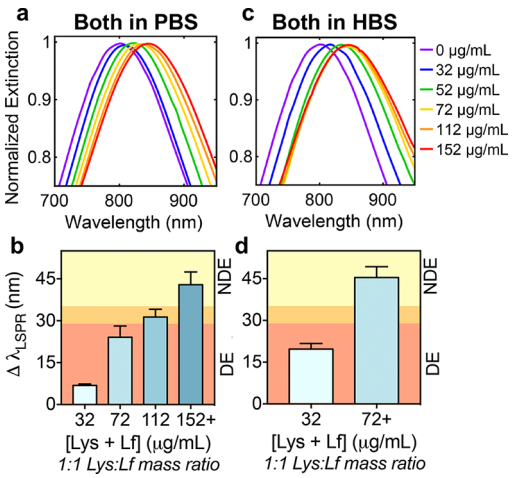

Figure 10. Analysis of LSPR shifts upon simultaneous variation of biomarker concentration in human tears. Gaussian fits to LSPR peaks of AuNS@PNM-normalized extinction spectra and quantitative analysis of shifts in LSPR of AuNS@PNM with increasing concentrations of both lysozyme (Lys) and lactoferrin (Lf) in either PBS or HBS. For clarity, Gaussian fits for high concentrations (*i.e.*, >96 μg/mL) were omitted. The shifts in LSPR in PBS (a,b) were smaller and showed a larger dynamic response across the concentrations tested compared with shifts observed in HBS (c,d). LSPR shifts that correspond to those of dry eye (DE) are represented by the red region, those that are borderline/additional testing recommended are represented by the orange region, and those that would be classified as non-dry eye (NDE) are represented by the yellow region (b,d). Data are reported as mean ± SD ($n \geq 3$).

DOI: 10.1021/acsnano.8b04348
ACS Nano XXXX, XXX, XXX−XXX

is further trained using samples from patients with chronic dry-eye conditions as well as age-matched, healthy controls.

Here, as an example of how measured LSPR shifts could be interpreted for diagnosing dry eye, we provide a discussion of the data assuming an idealized scenario, where the mass ratio of lysozyme and lactoferrin is 1:1 and the healthy concentration range for both proteins matches values reported in literature (Table 2). In this example, tears would be diluted 1/20 in PBS such that the concentrations in Figure 10b (32, 72, 112, and 152 μg/mL) would correspond to lysozyme + lactoferrin concentrations of approximately 0.64, 1.4, 2.2, and 3.0 mg/mL in the undiluted tears, respectively. The highest concentration (152 μg/mL in diluted tears or ~3.0 mg/mL in undiluted tears) falls within the normal range for healthy, non-dry-eye (NDE) subjects, the second highest concentration (112 μg/mL in diluted tears or ~2.2 mg/mL in undiluted tears) is at the lower end of what is considered healthy concentrations of both proteins, and the two lowest concentrations (32 and 72 μg/mL in diluted tears or ~0.64 and 1.4 mg/mL in undiluted tears, respectively) would be classified as abnormal, resulting in a dry-eye (DE) diagnosis. Thus, on the basis of the current data set, the LSPR shifts would be classified as follows: ≥35 nm = NDE (yellow region, Figure 10b,d), 29−35 nm = borderline/additional testing recommended (orange region, Figure 10b,d), and ≤29 nm = DE (red region, Figure 10b,d).

For AuNS@PNM in HBS, which quickly reached saturation when both lysozyme and lactoferrin concentrations were increased simultaneously (Figure 10c,d), higher dilutions (*e.g.*, 1/40) would be necessary to better distinguish among NDE, borderline, and DE levels of lysozyme and lactoferrin. Given these dilution factors, just 5 μL of tears, a reasonable volume to collect from patients with chronic dry eye, would be enough to perform multiple replicates using this LSPR-based assay.

We believe that by optimizing dilution factor, buffer, and AuNS@PNM concentration, it will be possible to use this single receptor to distinguish DE from NDE tears. However, if cross-reactivity turns out to be a problem when lysozyme and lactoferrin concentrations are unequal, then there are a few alternative approaches that could be considered: protein sequestration or differential sensing. In protein sequestration, careful buffer selection could be used to reduce competition. Specifically, if diluted tears were first incubated with AuNS@PNM in PBS, then we would expect lysozyme to occupy the binding sites first. Then, the AuNS@PNM with bound lysozyme could be removed *via* centrifugation, and the supernatant, which presumably would still have high lactoferrin concentration, could be buffer-exchanged into HBS and additional AuNS@PNM could be added to the HBS diluted tears, where binding between AuNS@PNM and lactoferrin is strong. Then, the LSPR shifts for both the first set of AuNS@PNM (in PBS, lysozyme-bound) and the second set of AuNS@PNM (in HBS, lactoferrin-bound) could be measured to obtain information about the concentrations of both biomarkers.

In differential sensing, a pattern is created from a suite of cross-reactive receptors to verify the presence of biomarkers in solution.[90] Moreover, the patterns can be used to analyze analyte concentrations, as well as the consistency of one biological mixture to the next (*e.g.*, human tears).[91,92] While in the present study we only used a single receptor, the synthesis scheme presented could be used to fabricate an array of receptors composed of additional ionic monomers as well as dynamic covalent monomers to enhance protein interaction and specificity. By expanding the number of receptors investigated (*i.e.*, hydrogel modified AuNSs of varying formulations), protein biomarkers tested, and buffers explored, differential sensing could be employed to extract a multitude of information about the tear composition and ultimately lead to a diagnostic platform for dry eye. Additionally, this technology could be adapted and applied to detect protein biomarkers present in other biological fluids to help diagnose additional diseases.

CONCLUSIONS

In this work, a method for synthesizing PNM, a protein-binding polymer, on the surface of AuNSs was developed. Additionally, the ability of these materials to serve as both molecular recognition and signal transduction agents was tested. Indeed, binding of two biomarkers of chronic dry eye, lysozyme and lactoferrin, caused large (up to 50 nm) shifts in the LSPR wavelength of AuNS@PNM. These large shifts enabled detection of clinically relevant concentrations of both protein biomarkers. Further training of the sensor with tears from individuals (both healthy and those with dry eye) will validate the potential for clinical translation as a rapid and affordable screening test for chronic dry eye and associated diseases.

METHODS

Materials. Poly(ethylene glycol) methacrylate (PEGMA) (MW of PEG block = 400) was purchased from Polysciences (Warrington, PA). Formaldehyde (Macron Fine Chemicals), 1 N sodium hydroxide, sodium chloride, 10× PBS, and FisherBrand Premium 1.5 mL polypropylene tubes were purchased from Thermo Fisher Scientific (Waltham, MA). Low adhesion centrifuge tubes were purchased from Andwin Scientific (Schaumburg, IL). Aminated silica nanoparticles (NPs) were purchased from (Nanocomposix, San Diego, CA). Ultrapure water (final resistance = 18.2 MΩ) was obtained from a Barnstead GenPure purification system from Thermo Fisher Scientific. Spectra/Por dialysis tubing was used for dialysis (12−14 kDa MWCO). Pooled human tears were purchased from Lee BioSolutions (Maryland Heights, MO). Human lysozyme and lactoferrin ELISA kits were purchased from Abcam (Cambridge, MA). All other reagents and proteins were purchased from Sigma-Aldrich (St. Louis, MO).

Synthesis of Poly(NIPAM-*co*-MAA) on PMAO-*g*-PEGMA-Stabilized Silica Gold Nanoshells. AuNSs were prepared based on previously described methods.[55,93] Details of the AuNS synthesis procedure are outlined in the Supporting Information because it was found that slight variations in the protocol can dramatically affect the quality of the prepared AuNSs. AuNS concentration was calculated based on a molar extinction coefficient of 2.6×10^{11} $M^{-1}cm^{-1}$ (estimated based on Mie theory calculations from Jain et al., specifically Figure 5b).[24] AuNSs (1.3 mL, 30 pM) were concentrated by centrifugation (1000*g*, 15 min) in low adhesion tubes (Andwin Scientific). The pellet was bath sonicated before adding 1 mL of PMAO-*g*-PEGMA in DI water (0.25 mg/mL, pH 7.4). Then, 20 μL of a 1% solution of DDT in ethanol was quickly added to the AuNSs and vortexed for 1 min. The PMAO-*g*-PEGMA-stabilized AuNSs (AuNS@PMAO-*g*-PEGMA) were allowed to sit at room temperature for 48 h, after which 600 μL of the supernatant was removed.

PNM was synthesized on the surface of AuNS@PMAO-*g*-PEGMA by adapting the precipitation polymerization procedure previously described for PNM.[20] The modifications to the procedure were the addition of the AuNS@PMAO-*g*-PEGMA in the polymerization mixture and modifying the percentage of *N*,*N*′-methylenebis-(acrylamide) (BIS) from 15 to 5 mol % relative to monomer. After polymerization, the samples were dialyzed at room temperature against nanopure water (800 mL) with at least six to eight water

DOI: 10.1021/acsnano.8b04348
ACS Nano XXXX, XXX, XXX−XXX

changes. The samples were then centrifuged at 1000*g* for 15 min and resuspended in water three to five times to concentrate AuNS@PNM and remove PNM nanogels without AuNS cores. AuNS@PNM were diluted to a concentration of ~5 pM (OD of ~0.3 for 20 μL in a 384-well plate). Synthesis was repeated in quadruplicate. Yield (based on volume required to reach the desired OD) was similar for batches 2–4 but low for batch 1.

Optimization of LSPR-Based Sensor. All LSPR spectra were measured using a BioTek Cytation 3 Cell Imaging Multi-Mode Plate Reader (BioTek Instruments). The sensitivity of AuNSs compared with AuNPs to refractive index changes was tested by measuring the absorbance spectra of both nanomaterials in solutions of different weight percent sucrose. The refractive indices of sucrose solutions are well-established and often used as refractive index standards.[56] AuNSs or AuNPs (made by the Turkevich method[94]) were combined with the sucrose solutions, and absorbance spectra were recorded. After determining the refractive index sensitivity of the AuNSs, AuNS@PNM and protein solutions in either 0.2× PBS (0.2× = 20 mM Na_2HPO_4, 3.6 mM KH_2PO4, 27.4 mM NaCl, 0.54 mM KCl, I = 34.6 mM, pH 7.4) or 0.2× HBS (0.2× = 5 mM L-histidine, 28 mM NaCl, I = 34.8 mM, pH 5.5) were combined in a 1:1 volume ratio in a 384-well plate for measuring absorbance spectra.

LSPR Sensing of Dry-Eye Biomarkers in Tears. Commercially available human ELISA kits (Abcam) were used to quantify the concentrations of lysozyme and lactoferrin in pooled human tears (Lee BioSolutions). Preparation and analysis of the ELISAs were performed according to the manufacturer's instructions. Human tears were diluted by a factor of 25 000 prior to use in the ELISA kit. Subsequent serial dilutions of the prepared tear solution were used to determine protein concentrations. Measurements were repeated in triplicate.

To vary the concentration of protein biomarkers individually, human tears were first diluted in either 0.2× HBS or 0.2× PBS to obtain an initial concentration of either lysozyme or lactoferrin at 16 μg/mL based on the ELISA results. Then, concentrated solutions of human lysozyme or human lactoferrin in 0.2× HBS or 0.2× PBS (1 mg/mL) were spiked into the respective buffered tear solutions to obtain final protein concentrations ranging from 16 to 216 μg/mL in 20 μg/mL increments. AuNS@PNM in water (5 pM) were combined with each protein solution at various concentrations at a 1:1 ratio in a 384-well plate (resultant path length = 2.3 mm). Each background-subtracted spectrum collected from these studies (from 650 to 950 nm) was fit to an eight-term Gaussian in MATLAB (version R2015b). Representative extinction spectra over the entire collected wavelength range (absolute, 400–1000 nm) and the Gaussian fit region (normalized, 650–950 nm) are shown in Figure S5. The LSPR wavelength was taken as the average of the centers of the Gaussians for at least three independently synthesized AuNS@PNM batches.

For studies where lysozyme and lactoferrin were varied simultaneously, human tears were diluted in either 0.2× HBS or 0.2× PBS to obtain an initial 16 μg/mL concentration of lactoferrin (at this concentration of lactoferrin in tears, lysozyme is present at ~8 μg/mL). A 3 mg/mL solution of human lysozyme in either 0.2× HBS or 0.2× PBS was prepared and added to the buffer diluted tear solution to obtain a working concentration of both lysozyme and lactoferrin at 16 μg/mL. The combined total protein concentration of lysozyme and lacterferrin was 32 μg/mL. Then, solutions of lysozyme and lactoferrin (1 mg/mL) in either 0.2× HBS or 0.2× PBS were prepared and added to the respective buffered tear solutions to obtain final total protein concentrations ranging from 32 to 432 μg/mL in 40 μg increments. AuNS@PNM in water was combined with each protein solution at various concentrations in a 1:1 ratio in a 384-well plate. Spectra collection and analysis was performed as previously mentioned.

Statistics. Absorbance measurements were repeated twice for at least three independently synthesized batches of AuNS@PNM, and results are presented as mean ± SD. Data comparing shifts in LSPR in 0.1× PBS *versus* 0.1× HBS were analyzed using Student's *t* tests. Data comparing shifts in LSPR in diluted tears for different protein concentrations were analyzed using multiple one-way ANOVAs in GraphPad Prism. Data were binned for protein concentrations where LSPR shifts were not statistically different.

ASSOCIATED CONTENT

Supporting Information

The Supporting Information is available free of charge on the ACS Publications website at DOI: 10.1021/acsnano.8b04348.

Detailed procedure for AuNS synthesis, DLS analysis, LSPR analysis for proteins of varied isoelectric point, ELISA analysis, table of all LSPR data for binding in human tears, and comparison of simultaneous *versus* individual variation of biomarker concentration (PDF)

AUTHOR INFORMATION

Corresponding Author

*E-mail: peppas@che.utexas.edu.

ORCID

Nicholas A. Peppas: 0000-0003-0894-5626

Present Address

#H.R.C.: Department of Chemical and Biological Engineering, University of Colorado Boulder, Boulder, CO, 80303, United States

Author Contributions

▽H.R.C. and M.E.W. contributed equally.

Notes

The authors declare no competing financial interest.

ACKNOWLEDGMENTS

Research reported in this publication was supported by the National Institute of Biomedical Imaging and Bioengineering of the National Institutes of Health under award number R01EB022025 (PIs: N.A.P. and E. Anslyn). In addition, N.A.P. acknowledges support from the Cockrell Family Chair Foundation, the office of the Dean of the Cockrell School of Engineering at the University of Texas at Austin (UT) for the Institute for Biomaterials, Drug Delivery, and Regenerative Medicine, and the UT-Portugal Collaborative Research Program. During this work, H.R.C. and M.E.W. were supported by National Science Foundation Graduate Research Fellowships (DGE-1610403). H.R.C. was also supported by a Donald D. Harrington Dissertation Fellowship. H.R.C. acknowledges the generous support of the Philanthropic Educational Organization Scholar Awards program. We thank L. Strong for input on AuNS synthesis and D. Romanovic for technical support with TEM.

REFERENCES

(1) Lee, D. W.; Neumann, P. J.; Rizzo, J. A. Understanding the Medical and Nonmedical Value of Diagnostic Testing. *Value Health* **2010**, *13*, 310–314.

(2) Giljohann, D. A.; Mirkin, C. A. Drivers of Biodiagnostic Development. *Nature* **2009**, *462*, 461–464.

(3) Turner, A. P. F. Biosensors: Sense and Sensibility. *Chem. Soc. Rev.* **2013**, *42*, 3184.

(4) Farid, S. S. Process Economics of Industrial Monoclonal Antibody Manufacture. *J. Chromatogr. B: Anal. Technol. Biomed. Life Sci.* **2007**, *848*, 8–18.

(5) Hueber, W.; Robinson, W. H. Proteomic Biomarkers for Autoimmune Disease. *Proteomics* **2006**, *6*, 4100–4105.

(6) Borrebaeck, C. A. Precision Diagnostics: Moving towards Protein Biomarker Signatures of Clinical Utility in Cancer. *Nat. Rev. Cancer* **2017**, *17*, 199.

DOI: 10.1021/acsnano.8b04348
ACS Nano XXXX, XXX, XXX–XXX

(7) Hermann, T.; Patel, D. J. Adaptive Recognition by Nucleic Acid Aptamers. *Science* **2000**, *287*, 820.
(8) Song, S.; Wang, L.; Li, J.; Fan, C.; Zhao, J. Aptamer-Based Biosensors. *TrAC, Trends Anal. Chem.* **2008**, *27*, 108−117.
(9) Zhou, J.; Battig, M. R.; Wang, Y. Aptamer-Based Molecular Recognition for Biosensor Development. *Anal. Bioanal. Chem.* **2010**, *398*, 2471−2480.
(10) Whitcombe, M. J.; Chianella, I.; Larcombe, L.; Piletsky, S. A.; Noble, J.; Porter, R.; Horgan, A. The Rational Development of Molecularly Imprinted Polymer-Based Sensors for Protein Detection. *Chem. Soc. Rev.* **2011**, *40*, 1547−1571.
(11) Mahon, C. S.; Jackson, A. W.; Murray, B. S.; Fulton, D. A. Investigating Templating within Polymer-Scaffolded Dynamic Combinatorial Libraries. *Polym. Chem.* **2013**, *4*, 368−377.
(12) Janiak, D. S.; Kofinas, P. Molecular Imprinting of Peptides and Proteins in Aqueous Media. *Anal. Bioanal. Chem.* **2007**, *389*, 399−404.
(13) Culver, H. R.; Peppas, N. A. Protein-Imprinted Polymers: The Shape of Things to Come? *Chem. Mater.* **2017**, *29*, 5753−5761.
(14) Culver, H. R.; Steichen, S. D.; Peppas, N. A. A Closer Look at the Impact of Molecular Imprinting on Adsorption Capacity and Selectivity for Protein Templates. *Biomacromolecules* **2016**, *17*, 4045−4053.
(15) Clegg, J. R.; Zhong, J. X.; Irani, A. S.; Gu, J.; Spencer, D. S.; Peppas, N. A. Characterization of Protein Interactions with Molecularly Imprinted Hydrogels That Possess Engineered Affinity for High Isoelectric Point Biomarkers. *J. Biomed. Mater. Res., Part A* **2017**, *105*, 1565−1574.
(16) Fredolini, C.; Meani, F.; Alex Reeder, K.; Rucker, S.; Patanarut, A.; Botterell, P. J.; Bishop, B.; Longo, C.; Espina, V.; Petricoin, E. F.; Liotta, L. A.; Luchini, A. Concentration and Preservation of Very Low Abundance Biomarkers in Urine, Such as Human Growth Hormone (HGH), by Cibacron Blue F3G-A Loaded Hydrogel Particles. *Nano Res.* **2008**, *1*, 502−518.
(17) Magni, R.; Espina, B. H.; Shah, K.; Lepene, B.; Mayuga, C.; Douglas, T. A.; Espina, V.; Rucker, S.; Dunlap, R.; Petricoin, E. F. I.; Kilavos, M. F.; Poretz, D. M.; Irwin, G. R.; Shor, S. M.; Liotta, L. A.; Luchini, A. Application of Nanotrap Technology for High Sensitivity Measurement of Urinary Outer Surface Protein A Carboxyl-Terminus Domain in Early Stage Lyme Borreliosis. *J. Transl. Med.* **2015**, *13*, 346.
(18) Yonamine, Y.; Hoshino, Y.; Shea, K. J. ELISA-Mimic Screen for Synthetic Polymer Nanoparticles with High Affinity to Target Proteins. *Biomacromolecules* **2012**, *13*, 2952−2957.
(19) Pelton, R. Temperature-Sensitive Aqueous Microgels. *Adv. Colloid Interface Sci.* **2000**, *85*, 1−33.
(20) Culver, H. R.; Sharma, I.; Wechsler, M. E.; Anslyn, E. V.; Peppas, N. A. Charged Poly(N-Isopropylacrylamide) Nanogels for Use as Differential Protein Receptors in a Turbidimetric Sensor Array. *Analyst* **2017**, *142*, 3183−3193.
(21) McClymer, J. P. Precise Determination of the Refractive Index of Suspended Particles: Light Transmission as a Function of Refractive Index Mismatch. *Am. J. Phys.* **2016**, *84*, 602−605.
(22) Willets, K. A.; Van Duyne, R. P. Localized Surface Plasmon Resonance Spectroscopy and Sensing. *Annu. Rev. Phys. Chem.* **2007**, *58*, 267−297.
(23) Anker, J. N.; Hall, W. P.; Lyandres, O.; Shah, N. C.; Zhao, J.; Van Duyne, R. P. Biosensing with Plasmonic Nanosensors. *Nat. Mater.* **2008**, *7*, 442−453.
(24) Jain, P. K.; Lee, K. S.; El-Sayed, I. H.; El-Sayed, M. A. Calculated Absorption and Scattering Properties of Gold Nanoparticles of Different Size, Shape, and Composition: Applications in Biological Imaging and Biomedicine. *J. Phys. Chem. B* **2006**, *110*, 7238−7248.
(25) Cao, J.; Sun, T.; Grattan, K. T. V. Gold Nanorod-Based Localized Surface Plasmon Resonance Biosensors: A Review. *Sens. Actuators, B* **2014**, *195*, 332−351.
(26) Jana, D.; Matti, C.; He, J.; Sagle, L. Capping Agent-Free Gold Nanostars Show Greatly Increased Versatility and Sensitivity for Biosensing. *Anal. Chem.* **2015**, *87*, 3964−3972.
(27) Takara, M.; Toyoshima, M.; Seto, H.; Hoshino, Y.; Miura, Y. Polymer-Modified Gold Nanoparticles *via* RAFT Polymerization: A Detailed Study for a Biosensing Application. *Polym. Chem.* **2014**, *5*, 931−939.
(28) Mesch, M.; Zhang, C.; Braun, P. V.; Giessen, H. Functionalized Hydrogel on Plasmonic Nanoantennas for Noninvasive Glucose Sensing. *ACS Photonics* **2015**, *2*, 475−480.
(29) Monteiro, J. P.; Predabon, S. M.; da Silva, C. T. P.; Radovanovic, E.; Girotto, E. M. Plasmonic Device Based on a PAAm Hydrogel/Gold Nanoparticles Composite. *J. Appl. Polym. Sci.* **2015**, *132*, 42449.
(30) Abbas, A.; Tian, L.; Morrissey, J. J.; Kharasch, E. D.; Singamaneni, S. Hot Spot-Localized Artificial Antibodies for Label-Free Plasmonic Biosensing. *Adv. Funct. Mater.* **2013**, *23*, 1789−1797.
(31) Luan, J.; Liu, K.-K.; Tadepalli, S.; Jiang, Q.; Morrissey, J. J.; Kharasch, E. D.; Singamaneni, S. PEGylated Artificial Antibodies: Plasmonic Biosensors with Improved Selectivity. *ACS Appl. Mater. Interfaces* **2016**, *8*, 23509−23516.
(32) Mayer, K. M.; Lee, S.; Liao, H.; Rostro, B. C.; Fuentes, A.; Scully, P. T.; Nehl, C. L.; Hafner, J. H. A Label-Free Immunoassay Based Upon Localized Surface Plasmon Resonance of Gold Nanorods. *ACS Nano* **2008**, *2*, 687−692.
(33) Tadepalli, S.; Kuang, Z.; Jiang, Q.; Liu, K.-K.; Fisher, M. A.; Morrissey, J. J.; Kharasch, E. D.; Slocik, J. M.; Naik, R. R.; Singamaneni, S. Peptide Functionalized Gold Nanorods for the Sensitive Detection of a Cardiac Biomarker Using Plasmonic Paper Devices. *Sci. Rep.* **2015**, *5*, 16206.
(34) Dong, P.; Lin, Y.; Deng, J.; Di, J. Ultrathin Gold-Shell Coated Silver Nanoparticles onto a Glass Platform for Improvement of Plasmonic Sensors. *ACS Appl. Mater. Interfaces* **2013**, *5*, 2392−2399.
(35) Aćimović, S. S.; Ortega, M. A.; Sanz, V.; Berthelot, J.; Garcia-Cordero, J. L.; Renger, J.; Maerkl, S. J.; Kreuzer, M. P.; Quidant, R. LSPR Chip for Parallel, Rapid, and Sensitive Detection of Cancer Markers in Serum. *Nano Lett.* **2014**, *14*, 2636−2641.
(36) Inci, F.; Tokel, O.; Wang, S.; Gurkan, U. A.; Tasoglu, S.; Kuritzkes, D. R.; Demirci, U. Nanoplasmonic Quantitative Detection of Intact Viruses from Unprocessed Whole Blood. *ACS Nano* **2013**, *7*, 4733−4745.
(37) Janssen, P. T.; van Bijsterveld, O. P. The Relations between Tear Fluid Concentrations of Lysozyme, Tear-Specific Prealbumin and Lactoferrin. *Exp. Eye Res.* **1983**, *36*, 773−779.
(38) Ohashi, Y.; Ishida, R.; Kojima, T.; Goto, E.; Matsumoto, Y.; Watanabe, K.; Ishida, N.; Nakata, K.; Takeuchi, T.; Tsubota, K. Abnormal Protein Profiles in Tears with Dry Eye Syndrome. *Am. J. Ophthalmol.* **2003**, *136*, 291−299.
(39) Hernández-Molina, G.; Sánchez-Hernández, T. Clinimetric Methods in Sjögren's Syndrome. *Semin. Arthritis Rheum.* **2013**, *42*, 627−639.
(40) Lin, H.; Yiu, S. C. Dry Eye Disease: A Review of Diagnostic Approaches and Treatments. *Saudi J. Ophthalmol.* **2014**, *28*, 173−181.
(41) Zeev, M. S.-B.; Miller, D. D.; Latkany, R. Diagnosis of Dry Eye Disease and Emerging Technologies. *Clin. Ophthalmol.* **2014**, *8*, 581−590.
(42) Phadatare, S. P.; Momin, M.; Nighojkar, P.; Askarkar, S.; Singh, K. K. A Comprehensive Review on Dry Eye Disease: Diagnosis, Medical Management, Recent Developments, and Future Challenges. *Adv. Pharm.* **2015**, *2015*, 1−12.
(43) D'Souza, S.; Tong, L. Practical Issues Concerning Tear Protein Assays in Dry Eye. *Eye Vis* **2014**, *1*, 6.
(44) Roy, N. S.; Wei, Y.; Kuklinski, E.; Asbell, P. A. The Growing Need for Validated Biomarkers and Endpoints for Dry Eye Clinical Research. *Invest. Ophthalmol. Visual Sci.* **2017**, *58*, BIO1−BIO19.
(45) Azkargorta, M.; Soria, J.; Acera, A.; Iloro, I.; Elortza, F. Human Tear Proteomics and Peptidomics in Ophthalmology: Toward the Translation of Proteomic Biomarkers into Clinical Practice. *J. Proteomics* **2017**, *150*, 359−367.
(46) Sambursky, R.; Davitt, W. F.; Latkany, R.; Tauber, S.; Starr, C.; Friedberg, M.; Dirks, M. S.; McDonald, M. Sensitivity and Specificity of a Point-of-Care Matrix Metalloproteinase 9 Immunoassay for

DOI: 10.1021/acsnano.8b04348
ACS Nano XXXX, XXX, XXX−XXX

Diagnosing Inflammation Related to Dry Eye. *JAMA Ophthalmol* **2013**, *131*, 24−28.
(47) Miller, M. A.; Rodrigues, M. A.; Glass, M. A.; Singh, S. K.; Johnston, K. P.; Maynard, J. A. Frozen-State Storage Stability of a Monoclonal Antibody: Aggregation Is Impacted by Freezing Rate and Solute Distribution. *J. Pharm. Sci.* **2013**, *102*, 1194−1208.
(48) Hutter, E.; Fendler, J. H. Exploitation of Localized Surface Plasmon Resonance. *Adv. Mater.* **2004**, *16*, 1685−1706.
(49) Lee, K.-S.; El-Sayed, M. A. Dependence of the Enhanced Optical Scattering Efficiency Relative to That of Absorption for Gold Metal Nanorods on Aspect Ratio, Size, End-Cap Shape, and Medium Refractive Index. *J. Phys. Chem. B* **2005**, *109*, 20331−20338.
(50) Chandra, K.; Culver, K. S. B.; Werner, S. E.; Lee, R. C.; Odom, T. W. Manipulating the Anisotropic Structure of Gold Nanostars Using Good's Buffers. *Chem. Mater.* **2016**, *28*, 6763−6769.
(51) Hrelescu, C.; Sau, T. K.; Rogach, A. L.; Jäckel, F.; Laurent, G.; Douillard, L.; Charra, F. Selective Excitation of Individual Plasmonic Hotspots at the Tips of Single Gold Nanostars. *Nano Lett.* **2011**, *11*, 402−407.
(52) Paulo, P. M. R.; Zijlstra, P.; Orrit, M.; Garcia-Fernandez, E.; Pace, T. C. S.; Viana, A. S.; Costa, S. M. B. Tip-Specific Functionalization of Gold Nanorods for Plasmonic Biosensing: Effect of Linker Chain Length. *Langmuir* **2017**, *33*, 6503−6510.
(53) Chen, H.; Kou, X.; Yang, Z.; Ni, W.; Wang, J. Shape- and Size-Dependent Refractive Index Sensitivity of Gold Nanoparticles. *Langmuir* **2008**, *24*, 5233−5237.
(54) Sun, Y.; Xia, Y. Increased Sensitivity of Surface Plasmon Resonance of Gold Nanoshells Compared to That of Gold Solid Colloids in Response to Environmental Changes. *Anal. Chem.* **2002**, *74*, 5297−5305.
(55) Oldenburg, S. J.; Averitt, R. D.; Westcott, S. L.; Halas, N. J. Nanoengineering of Optical Resonances. *Chem. Phys. Lett.* **1998**, *288*, 243−247.
(56) International Scale of Refractive Indices of Sucrose Solutions at 20 °C, 1936.
(57) Wu, C.; Xu, Q.-H. Stable and Functionable Mesoporous Silica-Coated Gold Nanorods as Sensitive Localized Surface Plasmon Resonance (LSPR) Nanosensors. *Langmuir* **2009**, *25*, 9441−9446.
(58) Nguyen, M.; Felidj, N.; Mangeney, C. Looking for Synergies in Molecular Plasmonics through Hybrid Thermoresponsive Nanostructures. *Chem. Mater.* **2016**, *28*, 3564−3577.
(59) Strong, L. E.; West, J. L. Hydrogel-Coated Near Infrared Absorbing Nanoshells as Light-Responsive Drug Delivery Vehicles. *ACS Biomater. Sci. Eng.* **2015**, *1*, 685−692.
(60) Song, J.; Yang, X.; Yang, Z.; Lin, L.; Liu, Y.; Zhou, Z.; Shen, Z.; Yu, G.; Dai, Y.; Jacobson, O.; Munasinghe, J.; Yung, B.; Teng, G.-J.; Chen, X. Rational Design of Branched Nanoporous Gold Nanoshells with Enhanced Physico-Optical Properties for Optical Imaging and Cancer Therapy. *ACS Nano* **2017**, *11*, 6102−6113.
(61) Lee, J.-E.; Chung, K.; Lee, J.; Shin, K.; Kim, D. H. *In Situ* Studies of Surface-Plasmon-Resonance-Coupling Sensor Mediated by Stimuli-Sensitive Polymer Linker. *Adv. Funct. Mater.* **2015**, *25*, 6716−6724.
(62) Joshi, G. K.; Smith, K. A.; Johnson, M. A.; Sardar, R. Temperature-Controlled Reversible Localized Surface Plasmon Resonance Response of Polymer-Functionalized Gold Nanoprisms in the Solid State. *J. Phys. Chem. C* **2013**, *117*, 26228−26237.
(63) Gehan, H.; Fillaud, L.; Chehimi, M. M.; Aubard, J.; Hohenau, A.; Felidj, N.; Mangeney, C. Thermo-Induced Electromagnetic Coupling in Gold/Polymer Hybrid Plasmonic Structures Probed by Surface-Enhanced Raman Scattering. *ACS Nano* **2010**, *4*, 6491−6500.
(64) Álvarez-Puebla, R. A.; Contreras-Cáceres, R.; Pastoriza-Santos, I.; Pérez-Juste, J.; Liz-Marzán, L. M. Au@pNIPAM Colloids as Molecular Traps for Surface-Enhanced, Spectroscopic, Ultra-Sensitive Analysis. *Angew. Chem.* **2009**, *121*, 144−149.
(65) Lim, S.; Song, J. E.; La, J. A.; Cho, E. C. Gold Nanospheres Assembled on Hydrogel Colloids Display a Wide Range of Thermoreversible Changes in Optical Bandwidth for Various Plasmonic-Based Color Switches. *Chem. Mater.* **2014**, *26*, 3272−3279.
(66) Contreras-Cáceres, R.; Sánchez-Iglesias, A.; Karg, M.; Pastoriza-Santos, I.; Pérez-Juste, J.; Pacifico, J.; Hellweg, T.; Fernández-Barbero, A.; Liz-Marzán, L. M. Encapsulation and Growth of Gold Nanoparticles in Thermoresponsive Microgels. *Adv. Mater.* **2008**, *20*, 1666−1670.
(67) Marcelo, G.; López-González, M.; Mendicuti, F.; Tarazona, M. P.; Valiente, M. Poly(*N* -Isopropylacrylamide)/Gold Hybrid Hydrogels Prepared by Catechol Redox Chemistry. Characterization and Smart Tunable Catalytic Activity. *Macromolecules* **2014**, *47*, 6028−6036.
(68) Yoon, M.; Lee, J.-E.; Jang, Y. J.; Lim, J. W.; Rani, A.; Kim, D. H. Comprehensive Study on the Controlled Plasmon-Enhanced Photocatalytic Activity of Hybrid Au/ZnO Systems Mediated by Thermoresponsive Polymer Linkers. *ACS Appl. Mater. Interfaces* **2015**, *7*, 21073−21081.
(69) Qian, Z.; Guye, K. N.; Masiello, D. J.; Ginger, D. S. Dynamic Optical Switching of Polymer/Plasmonic Nanoparticle Hybrids with Sparse Loading. *J. Phys. Chem. B* **2017**, *121*, 1092−1099.
(70) Yan, Y.; Liu, L.; Cai, Z.; Xu, J.; Xu, Z.; Zhang, D.; Hu, X. Plasmonic Nanoparticles Tuned Thermal Sensitive Photonic Polymer for Biomimetic Chameleon. *Sci. Rep.* **2016**, *6*, 31328.
(71) Culver, H. R.; Steichen, S. D.; Herrera-Alonso, M.; Peppas, N. A. Versatile Route to Colloidal Stability and Surface Functionalization of Hydrophobic Nanomaterials. *Langmuir* **2016**, *32*, 5629−5636.
(72) De Feijter, J. A.; Benjamins, J.; Veer, F. Ellipsometry as a Tool to Study Adsorption Behavior of Synthetic and Biopolymers at the Air-Water Interface. *Biopolymers* **1978**, *17*, 1759−1772.
(73) Wang, X.; Herting, G.; Odnevall Wallinder, I.; Blomberg, E. Adsorption of Bovine Serum Albumin on Silver Surfaces Enhances the Release of Silver at PH Neutral Conditions. *Phys. Chem. Chem. Phys.* **2015**, *17*, 18524−18534.
(74) Mazloomi-Rezvani, M.; Salami-Kalajahi, M.; Roghani-Mamaqani, H. Fabricating Core (Au)-Shell (Different Stimuli-Responsive Polymers) Nanoparticles *via* Inverse Emulsion Polymerization: Comparing DOX Release Behavior in Dark Room and under NIR Lighting. *Colloids Surf., B* **2018**, *166*, 144−151.
(75) Chakraborty, S.; Bishnoi, S. W.; Pérez-Luna, V. H. Gold Nanoparticles with Poly(*N* -Isopropylacrylamide) Formed *via* Surface Initiated Atom Transfer Free Radical Polymerization Exhibit Unusually Slow Aggregation Kinetics. *J. Phys. Chem. C* **2010**, *114*, 5947−5955.
(76) Wu, L.; Glebe, U.; Böker, A. Fabrication of Thermoresponsive Plasmonic Core-Satellite Nanoassemblies with a Tunable Stoichiometry *via* Surface-Initiated Reversible Addition-Fragmentation Chain Transfer Polymerization from Silica Nanoparticles. *Adv. Mater. Interfaces* **2017**, *4*, 1700092.
(77) Wu, T.; Zhang, Y.; Wang, X.; Liu, S. Fabrication of Hybrid Silica Nanoparticles Densely Grafted with Thermoresponsive Poly(*N*-Isopropylacrylamide) Brushes of Controlled Thickness *via* Surface-Initiated Atom Transfer Radical Polymerization. *Chem. Mater.* **2008**, *20*, 101−109.
(78) McGill, J. I.; Liakos, G. M.; Goulding, N.; Seal, D. V. Normal Tear Protein Profiles and Age-Related Changes. *Br. J. Ophthalmol.* **1984**, *68*, 316−320.
(79) Stuchell, R. N.; Feldman, J. J.; Farris, R. L.; Mandel, I. D. The Effect of Collection Technique on Tear Composition. *Ophthalmology* **1984**, *25*, 374−377.
(80) Balasubramanian, S. A.; Pye, D. C.; Willcox, M. D. P. Levels of Lactoferrin, Secretory IgA and Serum Albumin in the Tear Film of People with Keratoconus. *Exp. Eye Res.* **2012**, *96*, 132−137.
(81) You, J.; Fitzgerald, A.; Cozzi, P. J.; Zhao, Z.; Graham, P.; Russell, P. J.; Walsh, B. J.; Willcox, M.; Zhong, L.; Wasinger, V.; Li, Y. Post-Translation Modification of Proteins in Tears: Proteomics and 2-DE. *Electrophoresis* **2010**, *31*, 1853−1861.
(82) Versura, P.; Bavelloni, A.; Grillini, M.; Fresina, M.; Campos, E. C. Diagnostic Performance of a Tear Protein Panel in Early Dry Eye. *Mol. Vision* **2013**, *19*, 1247.

DOI: 10.1021/acsnano.8b04348
ACS Nano XXXX, XXX, XXX−XXX

(83) Fullard, R. J.; Tucker, D. L. Changes in Human Tear Protein Levels with Progressively Increasing Stimulus. *Invest. Ophthalmol. Visual Sci.* **1991**, *32*, 2290−2301.
(84) Martinez, R.; Acera, A.; Soria, J.; González, N.; Suárez, T. Allergic Mediators in Tear from Children with Seasonal and Perennial Allergic Conjunctivitis. *Arch. Soc. Esp. Oftalmol.* **2011**, *86*, 187−192.
(85) Massingale, M. L.; Li, X.; Vallabhajosyula, M.; Chen, D.; Wei, Y.; Asbell, P. A. Analysis of Inflammatory Cytokines in the Tears of Dry Eye Patients. *Cornea* **2009**, *28*, 1023.
(86) Ohashi, Y.; Dogru, M.; Tsubota, K. Laboratory Findings in Tear Fluid Analysis. *Clin. Chim. Acta* **2006**, *369*, 17−28.
(87) Niu, L.; Zhang, S.; Wu, J.; Chen, L.; Wang, Y. Upregulation of NLRP3 Inflammasome in the Tears and Ocular Surface of Dry Eye Patients. *PLoS One* **2015**, *10*, e0126277.
(88) Harris, D. C. *Quantitative Chemical Analysis*, 7th ed.; W. H. Freeman: New York, 2007.
(89) Vallée-Bélisle, A.; Ricci, F.; Plaxco, K. W. Engineering Biosensors with Extended, Narrowed, or Arbitrarily Edited Dynamic Range. *J. Am. Chem. Soc.* **2012**, *134*, 2876−2879.
(90) You, C.-C.; Miranda, O. R.; Gider, B.; Ghosh, P. S.; Kim, I.-B.; Erdogan, B.; Krovi, S. A.; Bunz, U. H. F.; Rotello, V. M. Detection and Identification of Proteins Using Nanoparticle−Fluorescent Polymer 'Chemical Nose' Sensors. *Nat. Nanotechnol.* **2007**, *2*, 318−323.
(91) Diehl, K. L.; Anslyn, E. V. Array Sensing Using Optical Methods for Detection of Chemical and Biological Hazards. *Chem. Soc. Rev.* **2013**, *42*, 8596.
(92) Lavigne, J. J.; Anslyn, E. V. Sensing a Paradigm Shift in the Field of Molecular Recognition: From Selective to Differential Receptors. *Angew. Chem., Int. Ed.* **2001**, *40*, 3118−3130.
(93) Strong, L. *Poly(NIPAAm-Co-AAm)-Gold Nanoshell Composites for Optically-Triggered Cancer Therapeutic Delivery*. Master Thesis, Rice University: Houston, TX, 2012.
(94) Turkevich, J.; Stevenson, P. C.; Hillier, J. A Study of the Nucleation and Growth Processes in the Synthesis of Colloidal Gold. *Discuss. Faraday Soc.* **1951**, *11*, 55.

DOI: 10.1021/acsnano.8b04348
ACS Nano XXXX, XXX, XXX−XXX